Title: High-risk microbial signatures are associated with severe parasitemia in controlled *Plasmodium* infections of both humans and rhesus macaques

Authors: Andrew T. Gustin[1,2], Courtney A. Broedlow[1,2,3], Kevin Hager[4,5], Ernesto Coronado[2,3], Solomon Wangari[2], Naoto Iwayama[2], Chul Y. Ahrens[2], William D. Garrison[2], Kathryn A. Guerriero[2,7], Kristina De Paris[8], Michael Gale, Jr.[1,2], Nichole R. Klatt[2,3,6], James G. Kublin[4], Jennifer A. Manuzak[2,3,9,10]

Affiliations:

[1]Department of Immunology, University of Washington, Seattle, WA, USA

[2]Washington National Primate Research Center, University of Washington, Seattle, WA, USA

[3]Department of Pharmaceutics, University of Washington, Seattle, WA, USA

[4]Seattle Malaria Clinical Trials Center, Fred Hutchinson Cancer Research Center, Seattle, Washington, USA

[5]Lumen Bioscience, Seattle, Washington, USA

[6]Division of Surgical Outcomes and Precision Medicine Research, Department of Surgery, University of Minnesota, Minneapolis, MN, USA

[7]Division of Veterinary Resources, National Institutes of Health Animal Center, Poolesville, MD, USA

[8]Department of Microbiology and Immunology, University of North Carolina School of Medicine, Chapel Hill, NC, USA

[9]Division of Immunology, Tulane National Primate Research Center, Tulane University, Covington, LA, USA

[10]Department of Microbiology and Immunology, Tulane University School of Medicine, New Orleans, LA, USA

***Corresponding author:**

Jennifer A. Manuzak

Assistant Professor

Division of Immunology

29 Tulane National Primate Research Center
30 Department of Microbiology and Immunology
31 Tulane University School of Medicine
32 18703 Three Rivers Road
33 Covington, LA, 70433
34 jmanuzak@tulane.edu
35
36 **Alternate corresponding author:**
37 Andrew T. Gustin
38 Postdoctoral scholar
39 Department of Immunology
40 University of Washington School of Medicine
41 750 Republican St.
42 Seattle, WA 98101
43 atgustin@uw.edu
44

45 **Abstract**

46 While functions of the gastrointestinal (GI) microbiome include maintenance of immune homeostasis and
47 protection against infectious disease, its role in determining disease severity during *Plasmodium* infection
48 has been limited to mouse models and observational human cohorts. Here, we performed controlled
49 *Plasmodium* infection in both humans and rhesus macaques (RMs) to experimentally determine the
50 impact of GI microbiome composition on disease progression. Through analysis of serially collected
51 microbiome samples, we identified a high-risk microbial signature that strongly associated with increased
52 risk of developing severe parasitemia in human participants. Importantly, we identified a parallel
53 phenomenon in RMs. The combined weight of this evidence demonstrates that pre-infection GI
54 microbiome composition is highly indicative of *P. falciparum* disease risk. Moreover, our observation that
55 *P. fragile*-microbiome dynamics in RMs closely mirrors *P. falciparum*-microbiome interactions in humans

56 strongly supports the use of this model in pre-clinical investigations of novel microbiome-targeting
57 approaches to reduce malaria burden.
58
59 **Introduction**
60 In 2020 there were 241 million cases of malaria worldwide, resulting in over 627,000 deaths[1]; leading
61 *Plasmodium* infection, the causative agent of malaria, to remain a significant global public health burden.
62 In addition to the classic clinical features of fever and anemia, *P. falciparum* malaria causes
63 gastrointestinal (GI) manifestations, including abdominal pain, diarrhea, and vomiting[2]. Moreover,
64 elevated GI *Plasmodium* parasite sequestration[3-6] causes damage to GI blood vessels and contributes
65 to disruptions in villi formation[7], and increased epithelial permeability[7,8], and malabsorption[9-11]. These
66 alterations may contribute to *Plasmodium*-induced microbial translocation[8,12-15] and dissemination of
67 nontyphoidal salmonella (NTS)[16,17]. However, the precise biological mechanisms underlying
68 *Plasmodium*-induced GI disruptions remain poorly defined.
69
70 GI microbes are essential in preserving epithelial barrier integrity and maintaining appropriate immune
71 surveillance; suboptimal GI microbial consortiums influence acquisition of enteric pathogens[18].
72 Interestingly, GI microbiome community structure may be linked with protection against severe
73 *Plasmodium* infection. Indeed, assessments of the fecal microbiota from Ugandan children suggest that
74 community composition varied between children that developed severe malaria anemia versus those with
75 asymptomatic *P. falciparum*[19]. Additionally, an observational study of children in Mali demonstrated that
76 time to *P. falciparum* infection was significantly delayed in those with higher stool abundances of
77 *Bifidobacterium* and *Streptococcus* species, suggesting an association between GI microbiome
78 composition and decreased prospective risk for *Plasmodium* acquisition[20]. In mice, higher GI abundances
79 of *Lactobacillus* and *Bifidobacterium* were associated with reduced parasite burden following *P. yoelii*
80 challenge[21], while decreased abundance of *Lactobacillaceae* and increased abundances of
81 *Enterobacteriaceae* and *Verrucomicrobiaceae* were inversely and positively correlated with *P. berghei*
82 ANKA burden, respectively[22]. Finally, differences in GI microbial communities in mice resistant or
83 susceptible to *P. yoelii* infection were associated with variations in the quality and specificity of spleen

84 anti-*Plasmodium* antibodies, providing a potential mechanism by which the GI microbiome could
85 influence the severity of *Plasmodium spp.* infection[23]. In sum, these findings support the notion that the
86 pre-existing GI microbiota composition may influence prospective risk for and severity of *Plasmodium*
87 infection.
88
89 While observational studies have linked microbiota composition and the prospective risk for and severity
90 of *Plasmodium* infection, there remains a critical need for controlled human malaria infection (CHMI)
91 studies to determine the role of the microbiome in shaping *Plasmodium* infection outcome. Such studies
92 will be important for determining whether previous cross-sectional and prospective findings are broadly
93 applicable across age ranges. Additionally, a representative animal model is required to assess
94 mechanistic relationships between *Plasmodium* infection and GI microbiota, intestinal inflammation, and
95 mucosal epithelial barrier integrity. While mouse models have provided useful insights, intervention-
96 based studies will likely require a non-human primate (NHP) model to assess the translational potential
97 of microbiota manipulation on malaria severity. Here, we present evidence from controlled malaria
98 infection studies in humans and NHPs that (1) confirms a strong relationship between pre-infection GI
99 microbiota composition and the potential for severe malaria; and (2) demonstrates that NHP are an ideal
100 animal model for basic and translational investigations of microbiome-*Plasmodium* interactions.
101
102 **Materials and Methods**
103 Controlled human malaria infection (CHMI) study and approval
104 Healthy adult participants were enrolled in a nonconfirmatory, 2-part, randomized, double-blinded,
105 placebo-controlled, single-center study completed at the Seattle Malaria Clinical Trials Center to test the
106 prophylactic efficacy, safety, and pharmacokinetics of KAF156, a novel imidazolopiperazine class of
107 antimalarial drug (clinical trials registration number: NCT04072302)[24]. As reported previously, KAF156
108 was found to be safe, well-tolerated, and resulted in a high degree of protective efficacy from *P.*
109 *falciparum* infection, which was tested through a controlled human malaria infection (CHMI) model[24]. A
110 subset of participants that received either placebo (n=8), 20mg (n=13), or 50mg (n=14) of KAF156 post-
111 CHMI exposure to *P. falciparum*-infected mosquitoes also provided stool samples at four distinct time

112 points: (1) within 1-2 days of CHMI; (2) during a three-day course of treatment with the antimalarial drug
113 Malarone (atovaquone/proguanil); (3) at the end of Malarone treatment; and (4) during CHMI and
114 treatment follow-up (within D28 – D42). *P. falciparum* infection in study participants was monitored in
115 whole peripheral blood using a *Plasmodium* 18S ribosomal RNA (rRNA) qRT-PCR that quantified Pf A-
116 type 18S rRNA[24-26]. Stool samples were frozen at -80°C within 24hours of collection. Upon thawing, DNA
117 was extracted from human stool samples and used for 16s rRNA sequencing analysis, as detailed below.
118

119 Nonhuman primate study animals, approval, and sample collection

120 Male Indian-origin rhesus macaques (*Macaca mulatta*; RMs; n=16) were housed and cared for at the
121 Washington National Primate Research Center (WaNPRC) under a protocol reviewed and approved by
122 the University of Washington Office of Animal Welfare (OWA) Institutional Animal Care and Use
123 Committee (IACUC; Protocol 4266-13; Animal Welfare Assurance Number D16-00292). The housing,
124 care, and procedures performed in this study were done in an AAALAC-accredited facility, in accordance
125 with the regulations put forth by the United States Department of Agriculture, including the Animal Welfare
126 Act (9 CRF) and the Animal Care Policy Manual, as well as with the guidelines outlined by the National
127 Research Council in the Guide for the Care and Use of Laboratory Animals and the Weatherall Report.
128 All RMs were provided with a commercial primate chow (Lab Diet, PMI Nutrition International, St. Louis,
129 MO) twice per day, supplemented with daily fruits and vegetables and water ad libitum. Novel food items,
130 foraging opportunities, and destructible and indestructible manipulanda were provided as environmental
131 enrichment. All RMs were housed in stainless steel cages with a 12/12 light cycle. All cage pans and
132 animal rooms were cleaned daily and sanitized at least every two weeks. Stool was collected from each
133 RM two weeks prior to *P. fragile* inoculation (Week -2), the day of *P. fragile* inoculation (Week 0), and
134 during *P. fragile* infection and treatment (Weeks 1, 2, 3, 4 and 6). The evening prior to stool collection,
135 RMs in full social contact were shifted into protected (grooming) contact only. The following morning,
136 stool was collected from each animal's cage pan and immediately stored at -80°C. Following cage pan
137 stool collection, RMs were returned to full social contact. Upon thawing, DNA was extracted from NHP
138 stool samples and used for 16s rRNA sequencing analysis.
139

140 *P. fragile* inoculation, post-infection monitoring, and treatment

141 *P. fragile*-infected RM erythrocytes were prepared as previously described[27]. Briefly, frozen erythrocytes
142 from a *P. fragile*-infected RM were thawed rapidly at 37°C and transferred into a sterile tube. Erythrocytes
143 were resuspended in 12% NaCl while gently shaking, followed by a 5min incubation at room temperature
144 without shaking. Next, 1.6% NaCl was added dropwise while gently shaking, followed by centrifugation
145 at 1400RPM, room temperature, 10min. After centrifugation, the supernatant was aspirated and
146 discarded, and the pellet resuspended in a solution of 0.9% NaCl and 2% dextrose, followed by
147 centrifugation at 1400RPM, room temperature, 10min. Finally, the supernatant was aspirated and
148 discarded, and the pellet resuspended in 0.9% NaCl solution. RMs were intravenously inoculated with up
149 to 20x10^6 *P. fragile*-infected erythrocytes in 1ml 0.9% NaCl solution.

150

151 Giemsa staining of thin blood smears was used to assess *P. fragile* parasitemia in each RM. Blood for
152 the smears was collected from non-sedated RMs using positive reinforcement conditioning. Parasitemia
153 checks occurred three times per week following *P. fragile* inoculation, with an additional check occurring
154 at week 6 post-*P. fragile* infection. Parasitemia was quantified using a light microscope and 1:10 ratio
155 Miller Disk Reticle (Microscope World, Carlsbad, CA), as previously described[28]. Briefly, the total number
156 of all red blood cells (RBCs), including both infected RBCs (iRBCs) and non-infected RBCs, inside the
157 minor square are enumerated, followed by counting of all iRBCs in the major square. A total of fifteen
158 fields were counted in three separate areas of the slide, for a total of 45 fields. The % parasitemia was
159 calculated in each of the three areas as follows: (# of iRBC in major square / # of all RBC in minor square)
160 x 10. The % parasitemia in each of the three areas was then averaged together to determine the final %
161 parasitemia for each RM at each timepoint.

162

163 The % parasitemia at each time point was used to determine the need for anti-malarial treatment. RMs
164 were treated using the following guidelines: if parasitemia was between 0.5-1%, RMs were treated orally
165 with quinine sulfate (150mg; NDC: 53489-0700-07; Sun Pharmaceuticals, Princeton, NJ) once per day.
166 If parasitemia was above 1%, RMs were treated orally with quinine sulfate twice per day. If parasitemia
167 was above 0.5% for two consecutive weeks despite quinine sulfate treatment, RMs were switched to oral

168 chloroquine treatment (10-20mg/kg; NDC: 64980-0178-02; Rising Pharmaceuticals, East Brunswick, NJ)
169 once per day. Quinine sulfate and chloroquine treatments were halted as soon as RMs were observed
170 to be below the 0.5% parasitemia threshold.
171
172 16s rRNA sequencing
173 DNA was extracted from both NHP and human stool samples using the PowerFecal DNA Isolation Kit
174 (Qiagen, Valencia, CA). Sequencing of the 16s small subunit ribosomal ribonucleic acid (SSU rRNA)
175 gene was performed at the University of Minnesota Genomics Center. Briefly, a quality control qPCR was
176 performed in triplicate to verify that sufficient quantities of the 16s SSU rRNA gene were present in the
177 sample for sequencing. After confirmation that adequate levels of the 16s SSU rRNA gene were
178 extracted, the following primers were used to sequence the V3/V4 region of the 16s SSU rRNA gene:
179 357F (5′-CCTACGGGNGGCAGCAG-3′) – 806R (5′-GGACTACNVGGGTWTCTAAT- 3′)[29-32]. Next, a
180 dual-indexing qPCR was used to barcode and add indexes for gene amplicon sequencing[33]. The resulting
181 amplicons were normalized, pooled, cleaned, and quantified (KAPA quantification, KAPA Biosystems,
182 Wilmington, MA). An Illumina MiSeq (Illumina, San Diego, CA) was used to sequence the library with a
183 2x300 bp cycle with 15% PhiX (Illumina). All raw sequence data have been deposited in the NCBI SRA
184 (accession number pending).
185
186 Bioinformatics and statistical analysis
187 16S rRNA amplicon sequencing reads were demultiplexed in Illumina Basespace. Fastq files were
188 assessed for read quality, trimmed (trimLeft=12, truncLen=150), dereplicated, and filtered using the
189 dada2 pipeline in R studio. Following removal of chimeric sequences, reads were assigned a taxonomy
190 using greengenes (gg_13_8_train_set_97.fa.gz) and a phylogenetic tree was built using MSA and
191 Phangorn. The reads, metadata, and tree were then combined into a phyloseq object for additional quality
192 controls and filtering, which included removing ASVs mapping to mitochondria, chloroplast and
193 cyanobacteria reads, as well as any ASV detected in only one sample. The resulting phyloseq object was
194 used for all downstream analyses.
195

196 Unsupervised hierarchical clustering was conducted on center log ratio (CLR)-transformed read counts,
197 using a divisive approach (Cluster::diana). The same CLR-transformed read counts were used to
198 visualize human reads in PCA space. Alpha diversity was calculated using the microbiome package to
199 assess raw reads. Prevalence, proportion tests, and CLR-transformed abundances were assessed using
200 custom scripts that are available upon request. Differential abundance was performed using DESeq2 to
201 assess raw reads on genera-level objects generated using phyloseq::tax_glom. Time course data were
202 smoothed using default options for ggplot2::geom_smooth. PCoA of RM samples were generated by first
203 running phyloseq::ordinate on the phyloseq object, and the resulting objects were visualized using
204 phyloseq::plot_ordination. All code is available upon request. Log2 peak parasite burdens, Shannon
205 diversity levels, and CLR-transformed counts were compared using a pairwise Wilcoxon test. Significant
206 differences in prevalence were assessed by proportion test. Differential abundances were determined
207 using DESeq2 with a Wald test.
208
209 **Results**
210 Pre-infection human microbiome composition is associated with parasite burden during controlled malaria
211 infection
212 We first assessed the stool microbiota in healthy adults participating in a CHMI study[24]. As previously
213 reported, study participants were inoculated via infected mosquito bite (n=35). Participants that
214 progressed to detectable parasitemia by qPCR (n=32) were included in the sequencing analysis
215 performed here[24]. Malarone (atovaquone/proguanil) treatment was initiated according to predetermined
216 criteria of two consecutive positive qRT-PCR test results, with at least one measurement greater than
217 250 parasites/ml[24]. Stool samples were collected (1) prior to challenge, (2) at peak parasitemia (prior to
218 antimalarial treatment thresholds), (3) post-treatment, and (4) during follow-up (Fig. 1A).
219
220 We hypothesized that the magnitude of *Plasmodium* parasite burden would vary according to microbiota
221 composition. To test this, we performed unsupervised, divisive hierarchical clustering of 16S rRNA gene
222 sequencing data to identify major community types. Baseline microbiota compositions could be
223 segregated into three distinct clusters (Fig.1B). We next categorized infection outcome as either mild or

224 severe parasitemia, defined as parasite burden above or below the median parasitemia value.
225 Participants in human microbiome cluster 1 (HC1; gold) were more than eight times as likely to
226 experience high parasitemia as HC3 participants (dark cyan; odds ratio (OR) = 8.17; p = 0.047; 95%
227 confidence interval (CI) = 1.03 – 64.94), while HC2 participants (gray) were more than four times as likely
228 to develop high parasitemia than HC3 participants (OR = 4.08; p = 0.149; 95% CI = 0.60 – 27.65) (Fig.
229 1C). When assessing parasite burden in each cluster, HC1 participants developed significantly higher
230 levels of parasitemia as compared to HC3 participants (p=0.043); HC1 peak parasitemia was also
231 elevated compared to HC2, although this difference did not reach statistical significance (p=0.17; Fig.
232 1D). Parasite burden was non-significantly elevated in HC2 compared to HC3 participants (p=0.23; Fig.
233 1D). Importantly, we observed no relationship between microbiome composition and post-exposure
234 treatment with KAF156 or placebo following *P. falciparum* challenge (Fig. S1A and B). Taken together,
235 microbiota composition prior to *P. falciparum* exposure was significantly associated with parasite burden
236 in humans.
237
238 <u>Human GI microbiome composition is robustly associated with malaria severity and progression</u>
239 We next identified structural and compositional distinctions between microbiota clusters by performing
240 components analysis (PCA) on all collected timepoints. HC1 participants were widely dispersed, HC2
241 participants were modestly dispersed, and HC3 participants were tightly clustered in PCA space (Fig. 2A
242 and B), indicating greater variability in microbial composition in HC1 than HC2 or HC3. These patterns
243 were especially evident with information from the third principal component added in 3-dimensional space
244 (Fig. S2A and B). When considering baseline only, HC2 and HC3 had significant overlap along PC1 and
245 minimal spread along PC2, while HC1 demonstrated higher variability along both PC axes (Fig. 2C and
246 D). These results affirmed the hierarchical cluster assignments by illustrating the degree to which HC1
247 differed from HC2 and HC3 in composition and variability at baseline and throughout *P. falciparum*
248 infection.
249
250 To determine whether within-sample alpha diversity was a distinguishing aspect of cluster identities, we
251 assessed the cumulative number of unique amplicon sequence variants (ASVs) detected at any time in

252 each microbiota cluster. The number of unique ASVs in HC1 (n=762) was almost two-fold greater than
253 in HC3 (n=488; Fig. 2E), indicating a greater range of taxa and explaining the wide dispersion of HC1
254 samples in PCA space. Additionally, HC1 Shannon diversity was elevated as compared to HC2, a finding
255 that remained stable across all measured time points and was statistically significant at baseline, post-
256 treatment, and follow-up (p=0.0011, 0.047, and 0.026, respectively; Fig. 2F). Likewise, measured
257 Shannon diversity in HC1 was significantly higher than HC3 at baseline and follow-up time points
258 (p=0.0021 and 0.00097, respectively; Fig. 2F). Shannon diversity scores for HC2 and HC3 participants
259 were similar over time, except follow-up where HC2 showed significantly higher scores than HC3
260 (p=0.025; Fig. 2F). Participants with high levels of parasitemia had consistently higher Shannon diversity
261 as compared to participants with mild parasitemia (Fig. 2G). This difference was statistically significant
262 pre-challenge (p=0.027) and trended towards significance at follow-up (p=0.054; Fig. 2G). Taken
263 together, elevated GI microbiota diversity prior to *P. falciparum* challenge could contribute to the
264 development of high parasitemia during infection. Additionally, stable diversity over time suggests that
265 pre-existing community structure is reestablished following transient changes induced by *Plasmodium*
266 infection.
267
268 <u>Genus-level distinctions in human intestinal microbial composition are linked with malaria disease</u>
269 <u>severity and progression</u>
270 To test whether the increased microbial richness in HC1 participants would result in reduced detection
271 and measured abundance of core ASCs compared to HC3 participants, we measured the prevalence of
272 all ASVs detected in at least one third of all participant samples at all time points and performed
273 proportionality tests. Highly prevalent ASVs, defined as ASVs detected in more than 75% of all samples,
274 were consistently detected at lower frequencies in HC1 than HC3 (Fig. 3A). Conversely, ASVs with lower
275 overall prevalence were more likely to be detected in HC1 than HC3. Among differentially prevalent ASVs,
276 several key GI microbiota were significantly less prevalent in HC1 participants, including *Bifidobacterium*
277 *longum* (p<0.0005), *Bifidobacterium adolescentis* (p<0.005), and *Akkermansia muciniphila* (p<0.005; Fig.
278 3A). We further assessed whether the abundances of core taxa, when detected, were different between
279 participant groups by comparing center log ratio (CLR)-transformed count data for the 20 most prevalent

280 taxa. Highly prevalent ASVs were significantly less abundant in HC1 participants as compared to HC2
281 and HC3 (Fig. 3B). The application of strict Bonferroni corrections demonstrated the strong significance
282 of this observation and highlighted reduced levels of *Bifidobacterium adolescentis* (p=0.00069; Fig. 3B).
283 Taken together, core GI microbiota ASVs are less prevalent and abundant in HC1 participants with high
284 parasite burdens, and their absence is accompanied by increased detection of low prevalence taxa.
285 These findings were robust even when accounting for decreased taxa prevalence.
286
287 To determine whether the risk for progression to severe malaria was driven by high-level community
288 composition differences, we performed differential abundance analysis on all pre-challenge samples at
289 the genus level. HC1 participants had reduced baseline levels of *Bifidobacterium*, *Streptococcus*, and
290 *Megamonas* relative to HC2 and HC3 participants (0.0067, 0.01, 0.0037, respectively; Fig 3C-F). These
291 reductions were balanced by increased levels of *Escherichia* and *Catenibacterium* (p=0.0016 and
292 <0.00001, respectively; Fig. 3C and G-H), among others. These baseline differences in community
293 composition were consistent throughout infection, with levels of *Megamonas* and *Bifidobacterium* stably
294 elevated in HC3, while *Blautia* and *Streptococcus* remained consistently highest in HC2, with HC3
295 approaching similar levels (Fig. 3I). Conversely, *Catenibacterium*, *Megasphaera*, *Peptoniphilius*, and
296 *WAL_1855D* were consistently elevated in HC1 (Fig. 3I), indicating a potential association with severe
297 malaria risk. *Escherichia* and *Roseburia* were disrupted following challenge, and although *Escherichia*
298 returned to pre-challenge levels in all community clusters*, Roseburia* was consistently diminished in HC3
299 following infection. Thus, high-level distinctions between microbiota clusters contributed to risk for malaria
300 severity, and GI microbial communities were generally stable subsequent to *P. falciparum* infection.
301
302 <u>Distinct RM microbial cluster is significantly associated with parasite burden during *P. fragile* infection</u>
303 To further test our hypothesis that the GI microbiome plays a direct role in *Plasmodium* progression, we
304 conducted experimental infection of rhesus macaques (RMs) with *P. fragile*, a macaque *Plasmodium*
305 previously shown to induce clinical signs in RMs comparable to those caused by *P. falciparum* in
306 humans[34-36]. Stool microbial communities of male RMs (n=16) were characterized two weeks prior to *P.*
307 *fragile* challenge and through six weeks post-infection (Fig. 4A). Unsupervised hierarchical clustering

308 revealed two major microbial community branches, macaque cluster 1 (MaC1) and 2 (MaC2). MaC1 RMs
309 were 21 times as likely to develop high parasite loads as MaC2 RMs (OR = 21.00; p = 0.024; 95%CI =
310 1.50-293.271). Moreover, MaC1 RMs reached peak parasite loads nearly three times greater than MaC2
311 RMs (p=0.003; Fig. 4C). Thus, the pre-infection microbiota composition of RMs was associated with the
312 likelihood of developing severe malaria, similarly to human CHMI participants.
313
314 RMs with distinct intestinal microbial composition have greater risk of developing severe malaria
315 As with CHMI data, PCA analyses reiterated the clear linkage between microbiota composition and
316 malaria progression (Figs. S3A and B). However, unlike CHMI participants, these distinctions were not
317 explained by alpha diversity differences. Indeed, Shannon diversity measurements indicated no
318 significant differences between MaC1 and MaC2 at any timepoint, nor were differences observed when
319 assessing Shannon diversity according to parasite burden (Fig. S3C and D), suggesting that distinctions
320 between RM microbiota clusters may not be driven by differences in community organization. We next
321 assessed community composition using PCoA of weighted-UniFrac values and found that MaC1
322 clustered separately from MaC2 (Fig. 5A) and displayed the clear association between microbiota
323 composition and parasite burden (Fig. 5B). Faceting data according to timepoint demonstrated that pre-
324 challenge microbial profiles remained distinct following recovery from *P. fragile* infection (Fig. 5C).
325 Notably, despite this overall stability, samples from week 3 post-challenge were not distinct in PCoA
326 space, suggesting that while microbial communities may be relatively resistant to influence from *P. fragile*
327 infection, they may be transiently disrupted (Fig. 5C). Taken together, our data demonstrate that parasite
328 burden was primarily driven by major compositional differences, rather than variable levels of microbiota
329 found in both groups.
330
331 Genus-level distinctions in RM intestinal microbial composition are linked with malaria disease severity
332 and progression
333 We next measured the abundance of core ASVs present in at least one third of all samples for each
334 microbiota cluster and performed proportionality tests (Fig. 6A). ASVs from the *Prevotella* genus and
335 *Ruminococcaea* family were more likely to be present in MaC2 RMs (Fig. 6A). Conversely, MaC1 RMs

336 more frequently carried ASVs from the *Lachnospiraceae* family, and the *Lactobacillus* and *Treponema*
337 genera (Fig. 6A). Notably, the majority of core ASVs had abundances that were relatively similar between
338 MaC1 and MaC2. Two important exceptions were the elevated abundance of several *Prevotella* ASVs in
339 MaC2 RMs, which were countered by significant elevations of *Lactobacillus* ASVs in MaC1 RMs (Fig.
340 6B). When assessing cumulative differences in ASVs at baseline, we identified 16 genera whose
341 abundances differed significantly between MaC1 and MaC2 (Fig. 6C). Interestingly, the *Prevotella* genus
342 was significantly elevated prior to challenge in MaC2 RMs (Fig. 6D), whereas MaC1 RMs had elevated
343 baseline levels of *Ruminococcus*, *Treponema*, and *Sphaerochaeta* (Fig. 6E-G). Finally, pre-challenge
344 elevations in *Prevotella* abundance in MaC2 were maintained over time (Fig. 6H), suggesting a beneficial
345 role of the *Prevotella* genus in the context of *Plasmodium* infection, as reduced levels were consistently
346 associated with the risk of severe parasitemia. Other genera shown to be significantly different pre-
347 challenge varied widely in abundance throughout *P. fragile* infection, with ratios between MaC1 and Mac2
348 frequently inverted during weeks 1 - 3 post-infection (Fig. 6B), the period during which parasite levels
349 were highest (Fig. S4). This observation agrees with our week-by-week breakdown of UniFrac distances
350 (Fig. 5C), indicating that *P. fragile* infection may disrupt the GI microbiome in RMs. Notably, the
351 abundance of most genera disrupted following *P. fragile* infection returned to pre-infection levels by 6
352 weeks post-challenge, thus reestablishing the distinction between MaC1 and MaC2 clusters. Taken
353 together, similarly to humans, RMs possess natural variation in GI microbiota that appears to predispose
354 a portion of the population to more severe *P. fragile* infection.
355

356 **Discussion**

357 Here, we observed that baseline GI microbiota composition in humans was strongly associated with the
358 potential for severe *P. falciparum* infection. Our findings are in agreement with observational studies
359 using incident detection in human children in malaria endemic areas[19,20] and previous murine studies[21-
360 23], both of which have suggested a link between GI microbiome composition and risk for severe malaria
361 infection. Importantly, our work extends these observations to adult humans and highlights
362 *Bifidobacterium* as a defining microbial feature in limiting risk for severe *P. falciparum* parasitemia. The
363 agreement between studies is impressive when considering that our CHMI study was performed on a

364 malaria-naïve cohort of adult individuals in Seattle, Washington, whereas the previous human studies
365 were conducted among infants and children in West Africa, where malaria incidence is seasonal. These
366 differences highlight the robust nature of our findings and position *Bifidobacterium* as a key taxon for
367 future studies aimed at mitigating malaria severity in endemic regions.
368
369 Our data suggest that elevated diversity in the GI microbiota prior to *P. falciparum* exposure could
370 contribute to the development of high parasitemia. Mechanistically, the loss or reduction of key
371 commensals including *Bifidobacterium* and *Akkermansia* could result in inappropriate or inadequate
372 priming of host immunity due to disruptions in beneficial, low-level immune stimulation[37-40]. Alternatively,
373 their displacement by an expansion of uncommon taxa could disturb GI metabolic networks and
374 subsequently promote pathologic changes to the GI barrier[41]. In either hypothetical, host immune
375 disruptions could manifest locally and systemically such that *Plasmodium* replication is promoted. Recent
376 work has also demonstrated a propensity for certain bacterial species to leverage within host evolution
377 to promote their translocation to the liver, altering immune homeostasis in this tissue[42]. Future
378 investigations focusing on the translocation potential of the differentially abundant taxa identified in this
379 study are needed. Alternatively, microbial composition may serve as a proxy for indirectly related facets
380 of overall health that may ultimately play larger roles in malaria progression; our identification of a similar
381 phenomenon in healthy RMs, however, argues against this. Finally, although unlikely, microbiome
382 constituents may directly impact the *Plasmodium* lifecycle. Future investigations to determine the precise
383 mechanisms by which GI microbiota composition influences the severity of *P. falciparum* infection in
384 humans are warranted.
385
386 As in humans, GI microbiota composition in RMs was significantly associated with severe *P. fragile*
387 parasitemia risk. In particular, pre-challenge differences in *Prevotella* between MaC1 and MaC2 were
388 maintained over time, suggesting that ASVs within this genus have a stable niche space that is diminished
389 in RMs likely to develop severe parasitemia. Notably, although the GI microbiome was generally resilient
390 to transient changes during *Plasmodium* infection in both humans and RMs, our data showed that when
391 disruptions occurred, they were observed near peak parasitemia. These findings are consistent with

392 previous work, which revealed only minimal differences in stool community structure and composition in
393 Kenyan infants before and after *P. falciparum* infection and treatment[43]. However, our data are in
394 opposition to murine studies which showed that *P. yoelli* infection resulted in decreased abundance of
395 Firmicutes and increased abundance of Bacteroidetes[5,44], while *P. berghei* ANKA infection resulted in
396 decreased Bacteroidetes and Verrucomicrobia phyla, but substantially increased Firmicutes and
397 Proteobacteria[45,46]. Taken together, the striking degree to which our RM GI microbiome findings agree
398 with both our CHMI data and prior human observational studies supports our hypothesis that microbiome
399 composition is a significant determining factor in *Plasmodium* infection. Moreover, our findings indicate
400 the significant translational potential of the RM *P. fragile* model. Given the additional strong similarities
401 between RMs and humans in terms of GI functionality and mucosal immunity, future studies utilizing this
402 model to investigate the impact of *P. fragile*-mediated GI microbiome disruptions on intestinal mucosal
403 barrier integrity and malaria disease progression are justified.
404
405 A major strength of our RM model is that it allowed for a greater degree of control over critical
406 experimental and population variables. Indeed, although our CHMI study employed narrowly defined
407 parameters for recruitment[24], there remained a potential for unassessed genetic, nutritional, and social
408 factors which may have contributed to microbiota variability. This created a challenge for determining
409 whether observed differences in baseline GI microbiota composition were a proxy for some other aspect
410 of *P. falciparum* susceptibility, or alternatively, played a direct role in risk for more severe infection. The
411 RM model allowed us to overcome some of these challenges, including the reduction of social, economic,
412 and medical confounders common among human cohorts. Additionally, while diet is a major contributor
413 to GI microbiota composition in both humans and RMs[47], the RMs included in this study were fed a
414 standardized diet of commercial primate chow and daily fruits and vegetables. Thus, while animal-to-
415 animal differences in GI microbiota composition prior to *P. fragile* challenge were expected, this variability
416 was unlikely to indicate unappreciated comorbidities or other factors that may have influenced *P. fragile*
417 infection. Moreover, the ability to stratify RMs according to pre-infection microbiota composition without
418 the added complications of needing to account for diet or other population-specific confounders,
419 strengthens our observation of a significant role of the GI microbiome in protection against severe

420 *Plasmodium* infection and verifies the value of this critical model system for the examination of
421 *Plasmodium*-microbiome interactions.
422
423 A critical aspect of our study was the use of an analytical approach that leveraged divisive hierarchal
424 clustering, as opposed to agglomerative, which enhanced our ability to segregate microbiota communities
425 into meaningful clusters. The ability to then identify stepwise increases in peak parasite burdens across
426 these microbiota clusters allowed us to verify previous studies suggesting an association between the
427 microbiome and the magnitude of *Plasmodium* infection, and extend these findings to a human adult
428 cohort, as well as a physiologically relevant RM model system. In sum, the data presented here and our
429 specific bioinformatic approach confirms the generalizability of our observations beyond specific
430 participant populations, as well as to other host and *Plasmodium* species.
431
432 In summary, the data presented here demonstrates that preexisting GI microbiome composition is highly
433 indicative of *Plasmodium* disease progression in humans and RMs. Our findings decisively support the
434 existence of a broad link between GI microbiome communities and *Plasmodium* infection severity and
435 represent a critical extension of previous murine and human studies[19-23] into adult human populations.
436 Our ability to recapitulate this phenomenon in a relevant RM model expands the ability to perform
437 mechanistic investigations of microbiota-influenced anti-malarial immunity. While our current study is
438 limited in its ability to make mechanistic determinations on how the GI microbiome contributes to
439 protection against severe malaria, the identification of high-level taxonomic differences in both human
440 and RM cohorts suggests that microbiome targeting therapies, such as microbiome modulation or small
441 molecule supplementation, could be investigated to mitigate the severity of *Plasmodium* infection. Taken
442 together, our data provide a strong foundation for future RM and human studies to identify the functional
443 role of distinct microbial communities in controlling malaria severity, and pre-clinically test preventative
444 and interventional strategies leveraging the microbiome to reduce malaria burden.
445
446 **Acknowledgements**

We thank the individuals that participated in the KAF156 CHMI study. We thank all veterinary and research support group staff of the Washington National Primate Research Center (WaNPRC) for their aid with the RM study. This work was supported by the resources and staff at the University of Minnesota Genomics Center. We thank Dr. Sheri Hild for her support of these studies.

Financial support

This work was supported by grant K01OD024876 to JAM, who was further supported in part by grants R21OD031435, R01HD108015, R01DA054553, and NIH base grant P51OD011104 to the Tulane National Primate Research Center. The research was additionally supported in part by WaNPRC NIH core grant P51OD010425. The KAF156 CHMI study was supported by Novartis.

Author contributions

JAM conceived of the study, oversaw the planning of the project, performed experiments, interpreted the data, and wrote the paper. ATG assisted with sample collection from the RM study, analyzed and interpreted the 16s rRNA sequencing data, and wrote the paper. CAB assisted with sample collection from the RM study and performed the DNA extractions and 16s rRNA sequencing for both the RM and CHMI studies. KH coordinated the collection of fecal samples from the CHMI study. EC provided support for sample processing from the RM study. SW, NI, CYA, and WDG provided research support for the RM study. KAG provided veterinary support for the RM study. KDP provided the initial *P. fragile* stock. MG and NRK assisted with data interpretation and paper preparation. JGK led and provided samples from the KAF156 CHMI study, assisted with data interpretation and paper preparation.

Conflicts of interest

All authors report no potential conflicts of interest.

Figure legends

Figure 1. Unsupervised hierarchical clustering of 16s rRNA sequences identifies association between GI microbiota composition and risk of severe *P. falciparum* parasitemia. (A)

475 Representative timeline depicting CHMI sample collection schedule. CHMI participants provided stool
476 samples near *P. falciparum* challenge (between days -2 – 2), at peak parasitemia near when treatment
477 was initiated (days 10 – 17), post-treatment (days 12 – 19), and at a follow-up visit (days 27 – 46). (B)
478 Divisive hierarchical clustering to identify major clusters in baseline microbiota samples. Major clusters
479 were defined as human cluster 1 (HC1; gold), human cluster 2 (HC2; gray) and human cluster 3 (HC3;
480 dark cyan). Branch tips indicate the parasitemia severity of each participant, which was based on
481 detection of peak parasite levels. (C) Odds ratio assessment to determine likelihood of participants within
482 each microbiota cluster progressing to severe parasitemia. (D) Log2-transformed parasitemia values for
483 participants in each microbiota cluster.
484
485 **Figure 2. High diversity GI microbiota is linked to likelihood of developing severe *P. falciparum***
486 **parasitemia.** (A) Principal component analysis (PCA) of CLR-transformed count data. Colors indicate
487 hierarchically determined microbiota clusters, with HC1 shown in gold, HC2 in gray, and HC3 in dark
488 cyan. (B) Replicate PCA as shown in A, with colors identifying samples associated with parasite levels.
489 Blue points indicate mild parasitemia, while red points indicate severe parasitemia. (C) PCA of samples
490 at baseline only, with points representative of HC1 (gold), HC2 (gray), and HC3 (dark cyan). (D) Replicate
491 PCA of samples at baseline only with points shaded to represent severe (red) and mild (blue) parasitemia.
492 (E) Total number of unique ASVs observed within each microbiota cluster. (F) Shannon diversity scores
493 for participant samples at all time points, grouped by microbiota cluster. (G) Shannon diversity scores for
494 participants at all time points, grouped by parasitemia severity.
495
496 **Figure 3. Abundance of core taxa is reduced in participants likely to develop severe *P. falciparum***
497 **parasitemia.** (A) Prevalence of all ASVs that were detected in at least one third of samples from each
498 microbiota cluster. Statistical values indicate significant differences in prevalence as determined by a
499 proportionality test. * = $p<0.05$, **=$p<0.005$, ***=$p<0.0005$. (B) CLR-transformed abundance data for top
500 20 most prevalent ASVs, when detected. Statistical significance between HC1 and HC3 was conducted
501 using a Wilcoxon test, with results that remained significant following Bonferroni correction boxed in dark
502 cyan. (C) Heatmap of CLR-transformed count data for all genera detected as differentially abundant at

503 the baseline time point, with hierarchical clustering of genera shown to the right. (D-H) CLR-transformed
504 counts for all baseline samples in select differentially abundant genera. (I) Smoothed abundance data
505 over time. Solid colored lines represent mean count levels. For panels A-B and D-I, HC1 is shown in gold,
506 HC2 is shown in gray and HC3 is shown in dark cyan.
507
508 **Figure 4. Unsupervised hierarchical clustering of 16s rRNA sequences identifies association**
509 **between GI microbiota composition and risk of severe *P. fragile* parasitemia.** (A) Representative
510 timeline depicting RM sample collection schedule. RM stool samples were collected twice prior to *P.*
511 *fragile* challenge, then each of the next four weeks, with final follow-up at six weeks post-challenge. (B)
512 Divisive hierarchical clustering to identify major clusters in baseline microbiota samples. Major clusters
513 were identified as macaque cluster 1 (MaC1; teal) and macaque cluster 2 (MaC2; purple). Branch tips
514 indicate the parasitemia severity of each macaque, which was based on detection of peak parasite levels.
515 (C) Log2-transformed parasitemia values for macaques in each microbiota cluster.
516
517 **Figure 5. GI microbiota composition linked to likelihood of developing severe *P. fragile***
518 **parasitemia.** (A) Principal Coordinate Analysis (PCoA) weighted-unifrac distances between samples.
519 Colors indicate hierarchically determined microbiota clusters, with MaC1 shown in teal and MaC2 shown
520 in purple. (B) Replicate PCoA as shown in (A), with colors identifying samples associated with parasite
521 levels. Blue points indicate mild parasitemia, while red points indicate severe parasitemia. (C) PCoA of
522 samples faceted by timepoint and colored by microbiota cluster.
523
524 **Figure 6. Abundance of core taxa reduced in macaques likely to develop severe *P. fragile***
525 **parasitemia.** (A) Prevalence of all ASVs that were detected in at least one third of samples from each
526 microbiota cluster. Statistical values indicate significant differences in prevalence as determined by a
527 proportionality test. * = $p<0.05$, **=$p<0.005$, ***=$p<0.0005$. (B) CLR-transformed abundance data for top
528 28 most prevalent ASVs, when detected. Statistical significance between MaC1 and MaC2 was
529 conducted using a Wilcoxon test, with results that remained significant following Bonferroni correction
530 boxed in teal when abundances were significantly greater in MaC1 and purple when abundances were

531 significantly greater in MaC2. (C) Heatmap of CLR-transformed count data for all genera detected as
532 differentially abundant at the baseline time point, with hierarchical clustering of genera shown to the right.
533 (D-E) CLR-transformed counts for all baseline samples in select differentially abundant genera. (F)
534 Smoothed abundance data over time. Solid colored lines represent mean count levels. For panels A-B
535 and D-F, MaC1 is shown in teal, MaC2 is shown in purple.
536
537 **Fig. S1. Post-CHMI treatment with KAF156 was not associated with microbiome composition.** (A)
538 Divisive hierarchical clustering to identify major clusters in baseline microbiota samples. Major clusters
539 were defined as human cluster 1 (HC1; gold), human cluster 2 (HC2; gray) and human cluster 3 (HC3;
540 dark cyan). Branch tips indicate the KAF156 treatment arm, including placebo (purple), 20mg (orange),
541 or 50mg (green) of KAF156 treatment post-CHMI. (B) Principal component analysis (PCA) of CLR-
542 transformed count data prior to challenge. Colors indicate the KAF156 treatment arm, including placebo
543 (purple), 20mg (orange), or 50mg (green) of KAF156 treatment post-CHMI.
544
545 **Fig. S2. High diversity human GI microbiota linked to likelihood of developing severe *P.*
546 *falciparum* parasitemia.** (A) Three-dimensional principal component analysis (PCA) of CLR-
547 transformed count data, with colors identifying samples associated with parasite levels. Blue points
548 indicate mild parasitemia, while red points indicate severe parasitemia. (B) Replicate PCA shown in (A),
549 with colors indicating hierarchically determined microbiota clusters. HC1 is shown in gold, HC2 is shown
550 in gray and HC3 is shown in dark cyan.
551
552 **Fig. S3. High diversity macaque GI microbiota linked to likelihood of developing severe *P.*
553 *falciparum* parasitemia.** (A) Principal component analysis (PCA) of CLR-transformed count data. Colors
554 indicate hierarchically determined microbiota clusters, with MaC1 shown in teal and MaC2 shown in
555 purple. (B) Replicate PCA shown in (A), with colors identifying samples associated with parasite levels.
556 Blue points indicate mild parasitemia, while red points indicate severe parasitemia. (C) Shannon diversity
557 scores for RM samples at all time points, grouped by microbiota cluster. (D) Shannon diversity scores for
558 RM samples at all time points, grouped by parasitemia severity.

559

560 **Fig. S4. Peak *P. fragile* parasite burdens varied across RMs.** (A) *P. fragile* parasite detection in

561 macaques over the study time course. Colors identify samples associated with parasite levels. Blue

562 background indicates RMs with mild parasitemia, while red points indicate RMs that experienced severe

563 parasitemia.

564

565

566 **References**

567

568 1 WHO. *World malaria report 2021*. Vol. Licence: CC BY-NC-SA 3.0 IGO (World Health
569 Organization, Geneva, Switzerland, 2021).
570 2 Sowunmi, A., Ogundahunsi, O. A., Falade, C. O., Gbotosho, G. O. & Oduola, A. M.
571 Gastrointestinal manifestations of acute falciparum malaria in children. *Acta tropica* **74**, 73-76
572 (2000).
573 3 Seydel, K. B., Milner, D. A., Jr., Kamiza, S. B., Molyneux, M. E. & Taylor, T. E. The distribution
574 and intensity of parasite sequestration in comatose Malawian children. *The Journal of infectious*
575 *diseases* **194**, 208-205 (2006). https://doi.org:10.1086/505078
576 4 Pongponratn, E., Riganti, M., Punpoowong, B. & Aikawa, M. Microvascular sequestration of
577 parasitized erythrocytes in human falciparum malaria: a pathological study. *The American journal*
578 *of tropical medicine and hygiene* **44**, 168-175 (1991).
579 5 Mooney, J. P. *et al.* Inflammation-associated alterations to the intestinal microbiota reduce
580 colonization resistance against non-typhoidal Salmonella during concurrent malaria parasite
581 infection. *Scientific reports* **5**, 14603 (2015). https://doi.org:10.1038/srep14603
582 6 Milner, D. A., Jr. *et al.* Quantitative Assessment of Multiorgan Sequestration of Parasites in Fatal
583 Pediatric Cerebral Malaria. *The Journal of infectious diseases* **212**, 1317-1321 (2015).
584 https://doi.org:10.1093/infdis/jiv205
585 7 Olsson, R. A. & Johnston, E. H. Histopathologic changes and small-bowel absorption in
586 falciparum malaria. *The American journal of tropical medicine and hygiene* **18**, 355-359 (1969).
587 8 Wilairatana, P., Meddings, J. B., Ho, M., Vannaphan, S. & Looareesuwan, S. Increased
588 gastrointestinal permeability in patients with Plasmodium falciparum malaria. *Clinical infectious*
589 *diseases : an official publication of the Infectious Diseases Society of America* **24**, 430-435 (1997).
590 9 Karney, W. W. & Tong, M. J. Malabsorption in Plasmodium falciparum malaria. *The American*
591 *journal of tropical medicine and hygiene* **21**, 1-5 (1972).
592 10 Molyneux, M. E. *et al.* Reduced hepatic blood flow and intestinal malabsorption in severe
593 falciparum malaria. *The American journal of tropical medicine and hygiene* **40**, 470-476 (1989).
594 11 Church, J. A., Nyamako, L., Olupot-Olupot, P., Maitland, K. & Urban, B. C. Increased adhesion of
595 Plasmodium falciparum infected erythrocytes to ICAM-1 in children with acute intestinal injury.
596 *Malaria Journal* **15**, 54 (2016). https://doi.org:10.1186/s12936-016-1110-3
597 12 Chau, J. Y. *et al.* Malaria-associated L-arginine deficiency induces mast cell-associated disruption
598 to intestinal barrier defenses against nontyphoidal Salmonella bacteremia. *Infection and immunity*
599 **81**, 3515-3526 (2013). https://doi.org:10.1128/iai.00380-13
600 13 Olupot-Olupot, P. *et al.* Endotoxaemia is common in children with Plasmodium falciparum malaria.
601 *BMC infectious diseases* **13**, 117 (2013). https://doi.org:10.1186/1471-2334-13-117
602 14 Berkley, J. A. *et al.* HIV infection, malnutrition, and invasive bacterial infection among children
603 with severe malaria. *Clinical infectious diseases : an official publication of the Infectious Diseases*
604 *Society of America* **49**, 336-343 (2009). https://doi.org:10.1086/600299

15 Bronzan, R. N. *et al.* Bacteremia in Malawian children with severe malaria: prevalence, etiology, HIV coinfection, and outcome. *The Journal of infectious diseases* **195**, 895-904 (2007). https://doi.org:10.1086/511437

16 Alamer, E. *et al.* Dissemination of non-typhoidal Salmonella during Plasmodium chabaudi infection affects anti-malarial immunity. *Parasitol Res* **118**, 2277-2285 (2019). https://doi.org:10.1007/s00436-019-06349-z

17 Potts, R. A. *et al.* Mast cells and histamine alter intestinal permeability during malaria parasite infection. *Immunobiology* **221**, 468-474 (2016). https://doi.org:10.1016/j.imbio.2015.11.003

18 Roth, A. N., Grau, K. R. & Karst, S. M. Diverse Mechanisms Underlie Enhancement of Enteric Viruses by the Mammalian Intestinal Microbiota. *Viruses* **11**, 760 (2019).

19 Mandal, R. K. *et al.* Dynamic modulation of spleen germinal center reactions by gut bacteria during Plasmodium infection. *Cell Rep* **35**, 109094 (2021). https://doi.org:10.1016/j.celrep.2021.109094

20 Yooseph, S. *et al.* Stool microbiota composition is associated with the prospective risk of Plasmodium falciparum infection. *BMC genomics* **16**, 631 (2015). https://doi.org:10.1186/s12864-015-1819-3

21 Villarino, N. F. *et al.* Composition of the gut microbiota modulates the severity of malaria. *Proceedings of the National Academy of Sciences of the United States of America* **113**, 2235-2240 (2016). https://doi.org:10.1073/pnas.1504887113

22 Taniguchi, T. *et al.* Plasmodium berghei ANKA causes intestinal malaria associated with dysbiosis. *Scientific reports* **5**, 15699 (2015). https://doi.org:10.1038/srep15699

23 Waide, M. L. *et al.* Gut Microbiota Composition Modulates the Magnitude and Quality of Germinal Centers during Plasmodium Infections. *Cell Rep* **33**, 108503 (2020). https://doi.org:10.1016/j.celrep.2020.108503

24 Kublin, J. G. *et al.* Safety, Pharmacokinetics, and Causal Prophylactic Efficacy of KAF156 in a Plasmodium falciparum Human Infection Study. *Clinical infectious diseases : an official publication of the Infectious Diseases Society of America* **73**, e2407-e2414 (2021). https://doi.org:10.1093/cid/ciaa952

25 Murphy, S. C., Daza, G., Chang, M. & Coombs, R. Laser cutting eliminates nucleic acid cross-contamination in dried-blood-spot processing. *Journal of clinical microbiology* **50**, 4128-4130 (2012). https://doi.org:10.1128/jcm.02549-12

26 Seilie, A. M. *et al.* Beyond Blood Smears: Qualification of Plasmodium 18S rRNA as a Biomarker for Controlled Human Malaria Infections. *The American journal of tropical medicine and hygiene* **100**, 1466-1476 (2019). https://doi.org:10.4269/ajtmh.19-0094

27 *Methods in malaria research*. 6th Edition edn, (EVIMalaR and MR4/ATCC, 2013).

28 Lim, C. *et al.* Improved light microscopy counting method for accurately counting Plasmodium parasitemia and reticulocytemia. *Am J Hematol* **91**, 852-855 (2016). https://doi.org:10.1002/ajh.24383

29 Sim, K. *et al.* Improved detection of bifidobacteria with optimised 16S rRNA-gene based pyrosequencing. *PloS one* **7**, e32543 (2012). https://doi.org:10.1371/journal.pone.0032543

30 Thompson, L. R. *et al.* A communal catalogue reveals Earth's multiscale microbial diversity. *Nature* **551**, 457-463 (2017). https://doi.org:10.1038/nature24621

31 Apprill, A., McNally, S., Parsons, R. & Weber, L. Minor revision to V4 region SSU rRNA 806R gene primer greatly increases detection of SAR11 bacterioplankton. *Aquatic Microbial Ecology* **75**, 129-137 (2015).

32 Caporaso, J. G. *et al.* Ultra-high-throughput microbial community analysis on the Illumina HiSeq and MiSeq platforms. *The ISME journal* **6**, 1621-1624 (2012). https://doi.org:10.1038/ismej.2012.8

33 Gohl, D. M. *et al.* Systematic improvement of amplicon marker gene methods for increased accuracy in microbiome studies. *Nature Biotechnology* **34**, 942-949 (2016). https://doi.org:10.1038/nbt.3601

34 Dissanaike, A., Nelson, P. & Garnham, P. Two New Malaria Parasites, *Plasmodium cynomolgi ceylonesis* subsp. nov and *Plasmodium fragile* sp. nov., from Monkeys in Ceylon. *Ceylon Journal of Medical Research*, 717-721 (1965).

35 Collins, W. E. *et al.* Studies on sporozoite-induced and chronic infections with Plasmodium fragile in Macaca mulatta and New World monkeys. *J Parasitol* **92**, 1019-1026 (2006). https://doi.org:10.1645/ge-848r.1

36 Collins, W. E., Chin, W. & Skinner, J. C. Plasmodium fragile and Macaca mulatta monkeys as a model system for the study of malaria vaccines. *The American journal of tropical medicine and hygiene* **28**, 948-954 (1979). https://doi.org:10.4269/ajtmh.1979.28.948

37 Abt, M. C. *et al.* Commensal bacteria calibrate the activation threshold of innate antiviral immunity. *Immunity* **37**, 158-170 (2012). https://doi.org:10.1016/j.immuni.2012.04.011

38 Brown, R. L., Sequeira, R. P. & Clarke, T. B. The microbiota protects against respiratory infection via GM-CSF signaling. *Nature communications* **8**, 1512 (2017). https://doi.org:10.1038/s41467-017-01803-x

39 Ganal, S. C. *et al.* Priming of natural killer cells by nonmucosal mononuclear phagocytes requires instructive signals from commensal microbiota. *Immunity* **37**, 171-186 (2012). https://doi.org:10.1016/j.immuni.2012.05.020

40 Hensley-McBain, T. *et al.* Increased mucosal neutrophil survival is associated with altered microbiota in HIV infection. *PLoS pathogens* **15**, e1007672 (2019). https://doi.org:10.1371/journal.ppat.1007672

41 Rooks, M. G. & Garrett, W. S. Gut microbiota, metabolites and host immunity. *Nat Rev Immunol* **16**, 341-352 (2016). https://doi.org:10.1038/nri.2016.42

42 Yang, Y. *et al.* Within-host evolution of a gut pathobiont facilitates liver translocation. *Nature* **607**, 563-570 (2022). https://doi.org:10.1038/s41586-022-04949-x

43 Mandal, R. K. *et al.* Longitudinal Analysis of Infant Stool Bacteria Communities Before and After Acute Febrile Malaria and Artemether-Lumefantrine Treatment. *The Journal of infectious diseases* **220**, 687-698 (2019). https://doi.org:10.1093/infdis/jiy740

44 Guan, W. *et al.* Observation of the Gut Microbiota Profile in BALB/c Mice Induced by Plasmodium yoelii 17XL Infection. *Frontiers in microbiology* **13**, 858897 (2022). https://doi.org:10.3389/fmicb.2022.858897

45 Guan, W. *et al.* Observation of the Gut Microbiota Profile in C57BL/6 Mice Induced by Plasmodium berghei ANKA Infection. *Frontiers in cellular and infection microbiology* **11**, 680383 (2021). https://doi.org:10.3389/fcimb.2021.680383

46 Fan, Z. G. *et al.* Gut Microbiota Reconstruction Following Host Infection with Blood-stage Plasmodium berghei ANKA Strain in a Murine Model. *Curr Med Sci* **39**, 883-889 (2019). https://doi.org:10.1007/s11596-019-2119-y

47 Zmora, N., Suez, J. & Elinav, E. You are what you eat: diet, health and the gut microbiota. *Nature reviews. Gastroenterology & hepatology* **16**, 35-56 (2019). https://doi.org:10.1038/s41575-018-0061-2

Figure 1

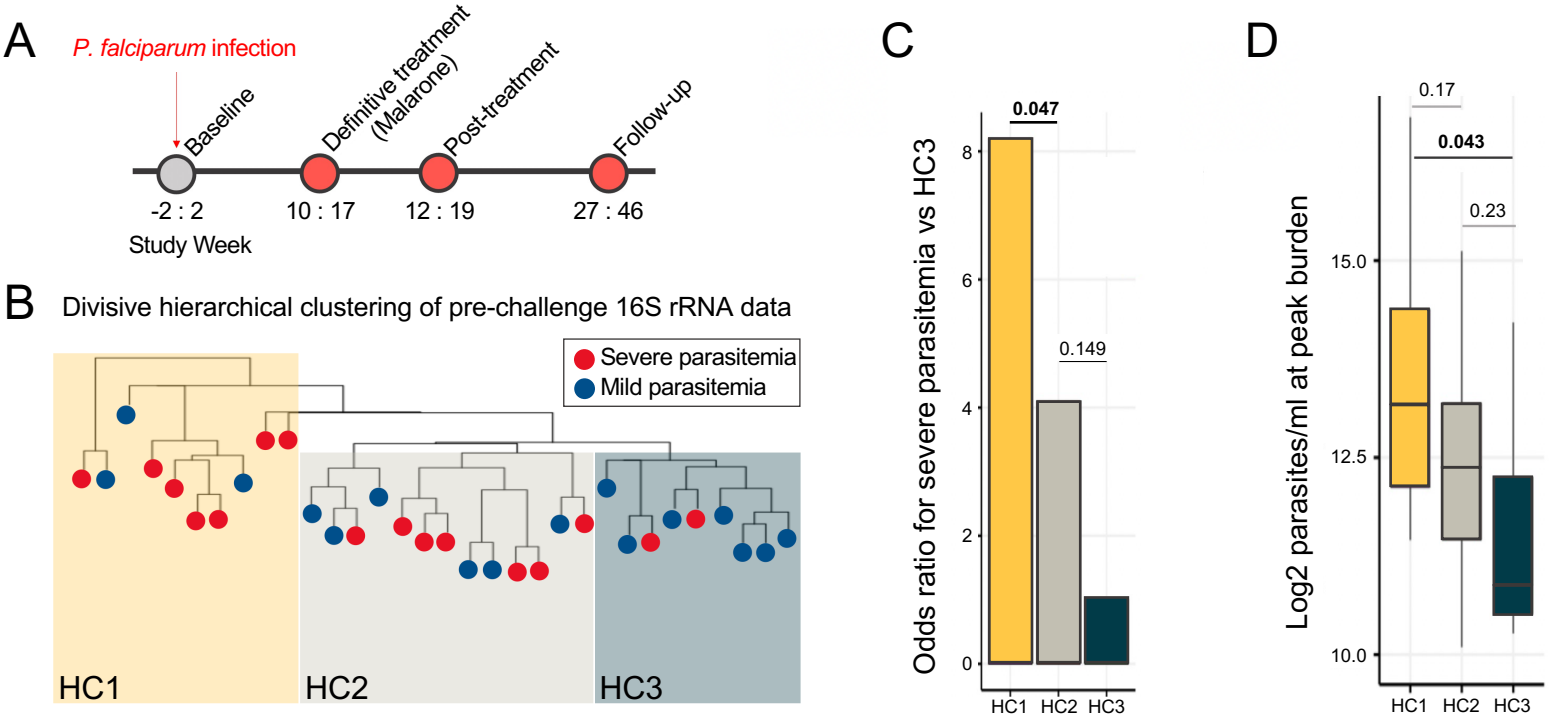
A
P. falciparum infection
Baseline
Definitive treatment (Malarone)
Post-treatment
Follow-up
-2 : 2
10 : 17
12 : 19
27 : 46
Study Week
B
Divisive hierarchical clustering of pre-challenge 16S rRNA data
Severe parasitemia
Mild parasitemia
HC1
HC2
HC3
C
Odds ratio for severe parasitemia vs HC3
0.047
0.149
HC1
HC2
HC3
D
Log2 parasites/ml at peak burden
0.17
0.043
0.23
HC1
HC2
HC3

Figure 2

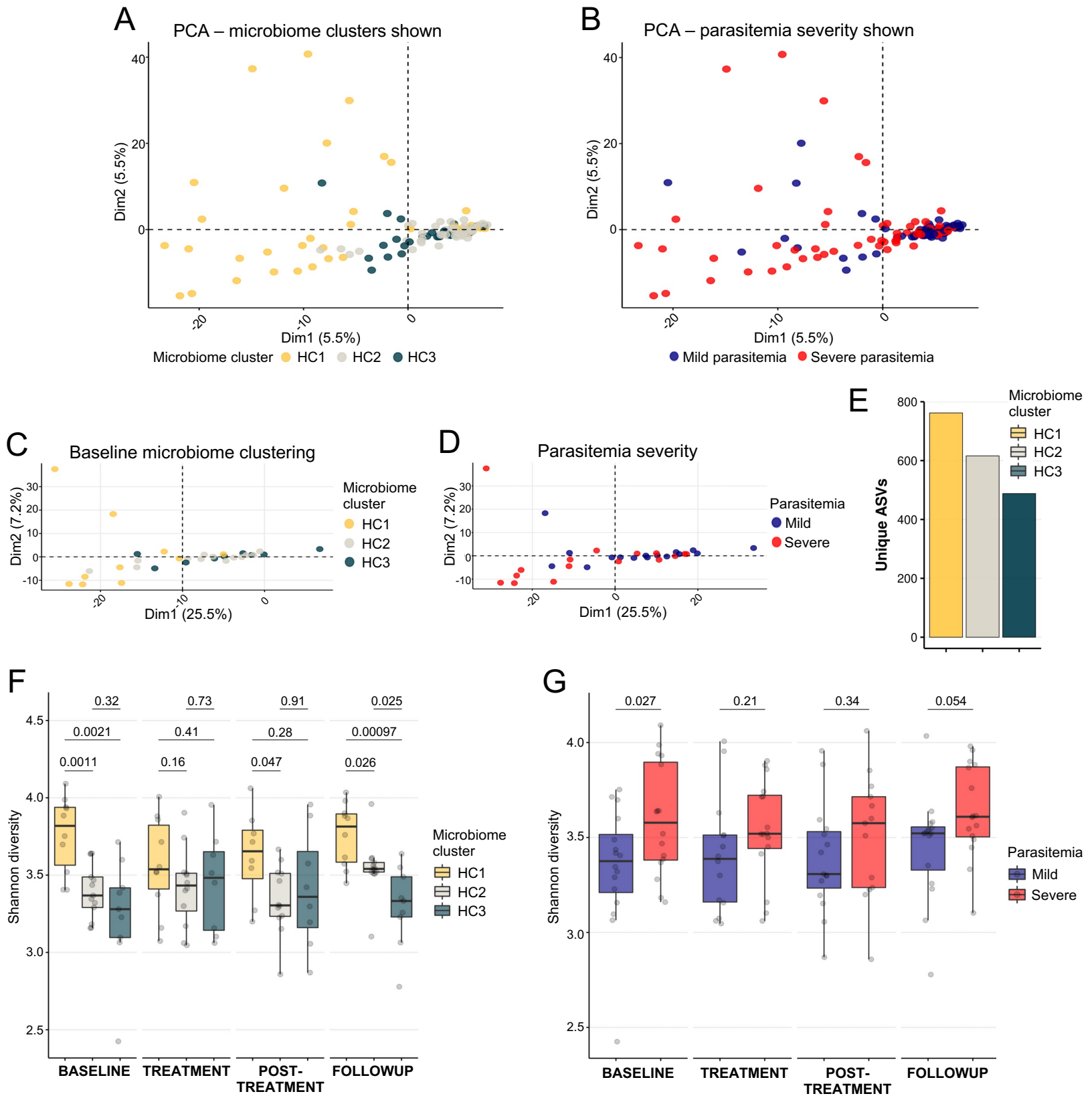
A
PCA – microbiome clusters shown
Dim2 (5.5%)
Dim1 (5.5%)
Microbiome cluster HC1 HC2 HC3
B
PCA – parasitemia severity shown
Dim2 (5.5%)
Dim1 (5.5%)
Mild parasitemia Severe parasitemia
C
Baseline microbiome clustering
Dim2 (7.2%)
Dim1 (25.5%)
Microbiome cluster
HC1
HC2
HC3
D
Parasitemia severity
Dim2 (7.2%)
Dim1 (25.5%)
Parasitemia
Mild
Severe
E
Unique ASVs
Microbiome cluster
HC1
HC2
HC3
F
Shannon diversity
0.32
0.73
0.91
0.025
0.0021
0.41
0.28
0.00097
0.0011
0.16
0.047
0.026
BASELINE
TREATMENT
POST-TREATMENT
FOLLOWUP
Microbiome cluster
HC1
HC2
HC3
G
Shannon diversity
0.027
0.21
0.34
0.054
BASELINE
TREATMENT
POST-TREATMENT
FOLLOWUP
Parasitemia
Mild
Severe

Figure 3

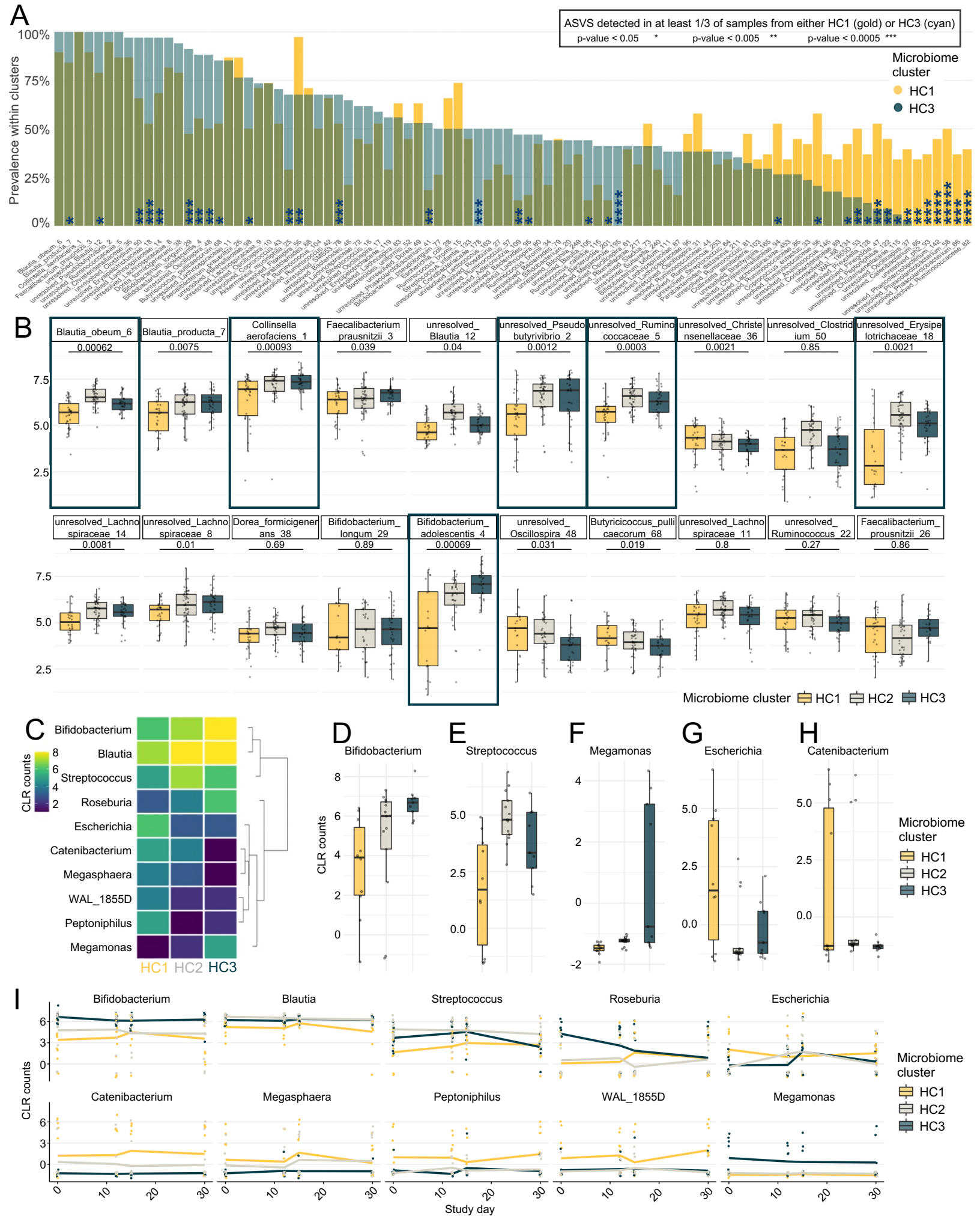
A
ASVS detected in at least 1/3 of samples from either HC1 (gold) or HC3 (cyan)
p-value < 0.05 *
p-value < 0.005 **
p-value < 0.0005 ***
Prevalence within clusters
100%
75%
50%
25%
0%
Microbiome cluster
HC1
HC3
B
Blautia_obeum_6
0.00062
Blautia_producta_7
0.0075
Collinsella_aerofaciens_1
0.00093
Faecalibacterium_prausnitzii_3
0.039
unresolved_Blautia_12
0.04
unresolved_Pseudobutyrivibrio_2
0.0012
unresolved_Ruminococcaceae_5
0.0003
unresolved_Christensenellaceae_36
0.0021
unresolved_Clostridium_50
0.85
unresolved_Erysipelotrichaceae_18
0.0021
unresolved_Lachnospiraceae_14
0.0081
unresolved_Lachnospiraceae_8
0.01
Dorea_formicigenerans_38
0.69
Bifidobacterium_longum_29
0.89
Bifidobacterium_adolescentis_4
0.00069
unresolved_Oscillospira_48
0.031
Butyricicoccus_pullicaecorum_68
0.019
unresolved_Lachnospiraceae_11
0.8
unresolved_Ruminococcus_22
0.27
Faecalibacterium_prausnitzii_26
0.86
7.5
5.0
2.5
Microbiome cluster HC1 HC2 HC3
C
Bifidobacterium
Blautia
Streptococcus
Roseburia
Escherichia
Catenibacterium
Megasphaera
WAL_1855D
Peptoniphilus
Megamonas
CLR counts
8
6
4
2
HC1 HC2 HC3
D
Bifidobacterium
E
Streptococcus
F
Megamonas
G
Escherichia
H
Catenibacterium
CLR counts
Microbiome cluster
HC1
HC2
HC3
I
Bifidobacterium
Blautia
Streptococcus
Roseburia
Escherichia
Catenibacterium
Megasphaera
Peptoniphilus
WAL_1855D
Megamonas
CLR counts
Study day
0
10
20
30

Figure 4

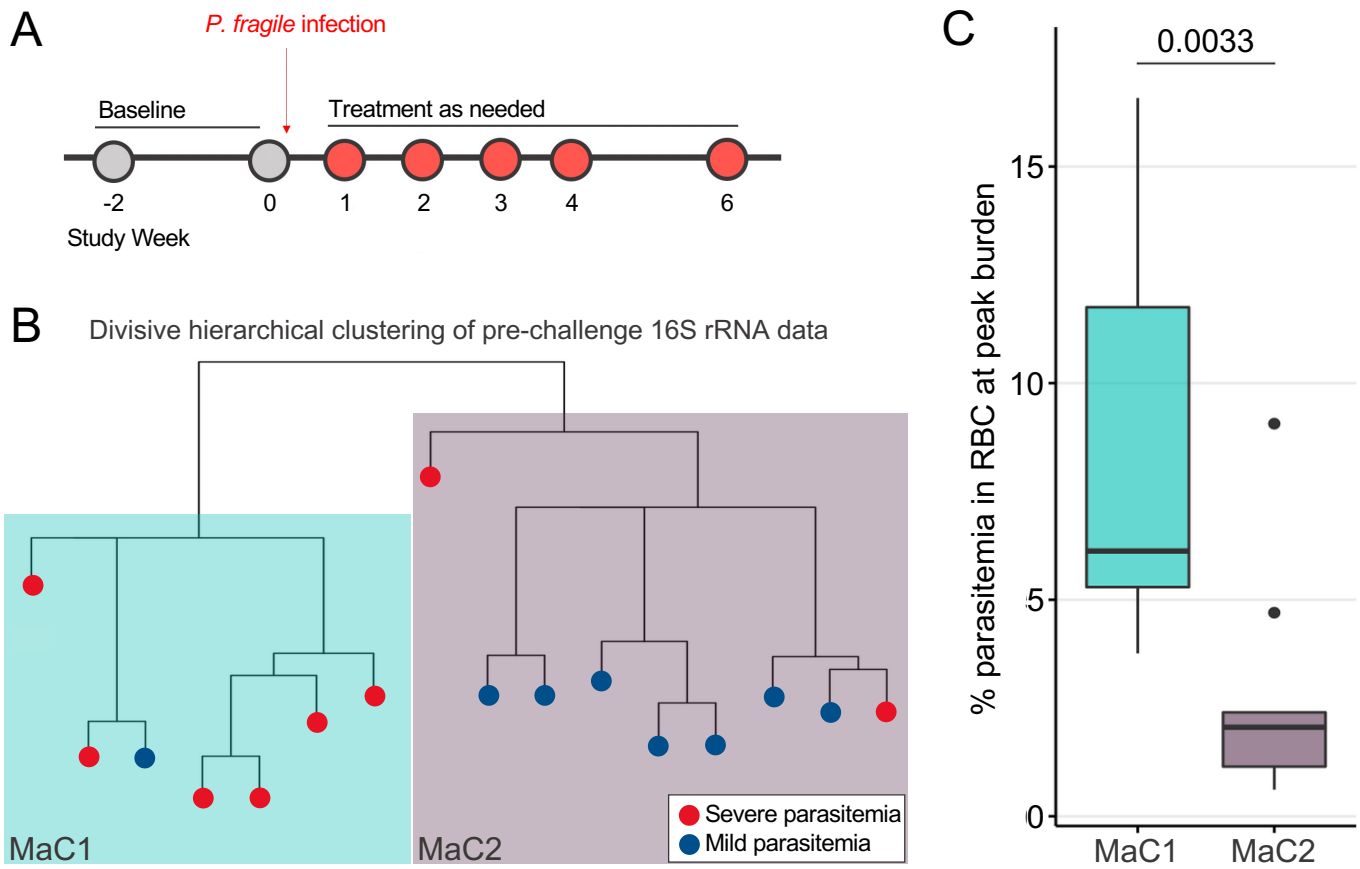
A
P. fragile infection
Baseline
Treatment as needed
-2
0
1
2
3
4
6
Study Week
B
Divisive hierarchical clustering of pre-challenge 16S rRNA data
MaC1
MaC2
Severe parasitemia
Mild parasitemia
C
0.0033
% parasitemia in RBC at peak burden
15
10
5
0
MaC1
MaC2

Figure 5

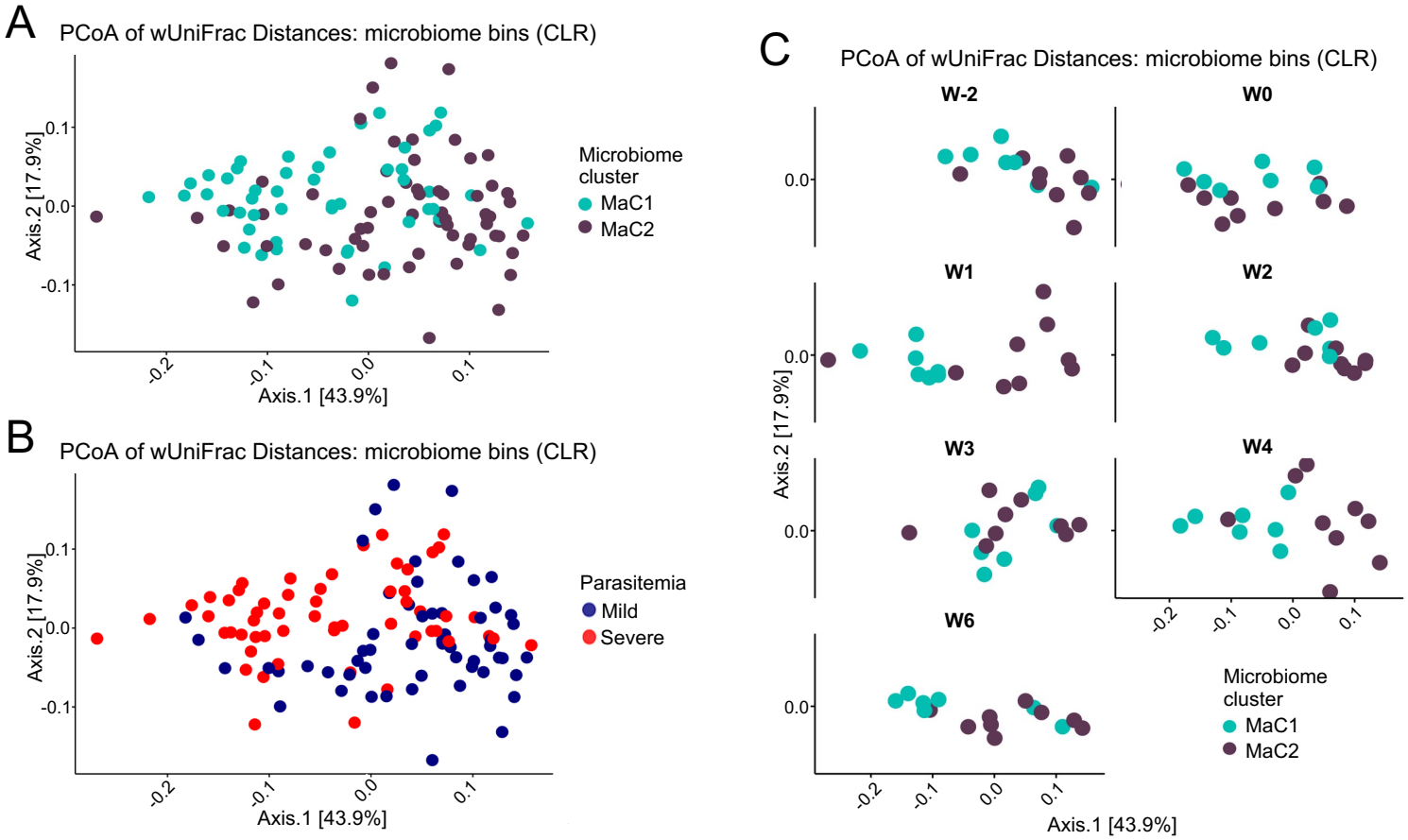
A
PCoA of wUniFrac Distances: microbiome bins (CLR)
Axis.2 [17.9%]
Axis.1 [43.9%]
Microbiome cluster
MaC1
MaC2
B
PCoA of wUniFrac Distances: microbiome bins (CLR)
Axis.2 [17.9%]
Axis.1 [43.9%]
Parasitemia
Mild
Severe
C
PCoA of wUniFrac Distances: microbiome bins (CLR)
W-2
W0
W1
W2
W3
W4
W6
Axis.2 [17.9%]
Axis.1 [43.9%]
Microbiome cluster
MaC1
MaC2

Figure 6

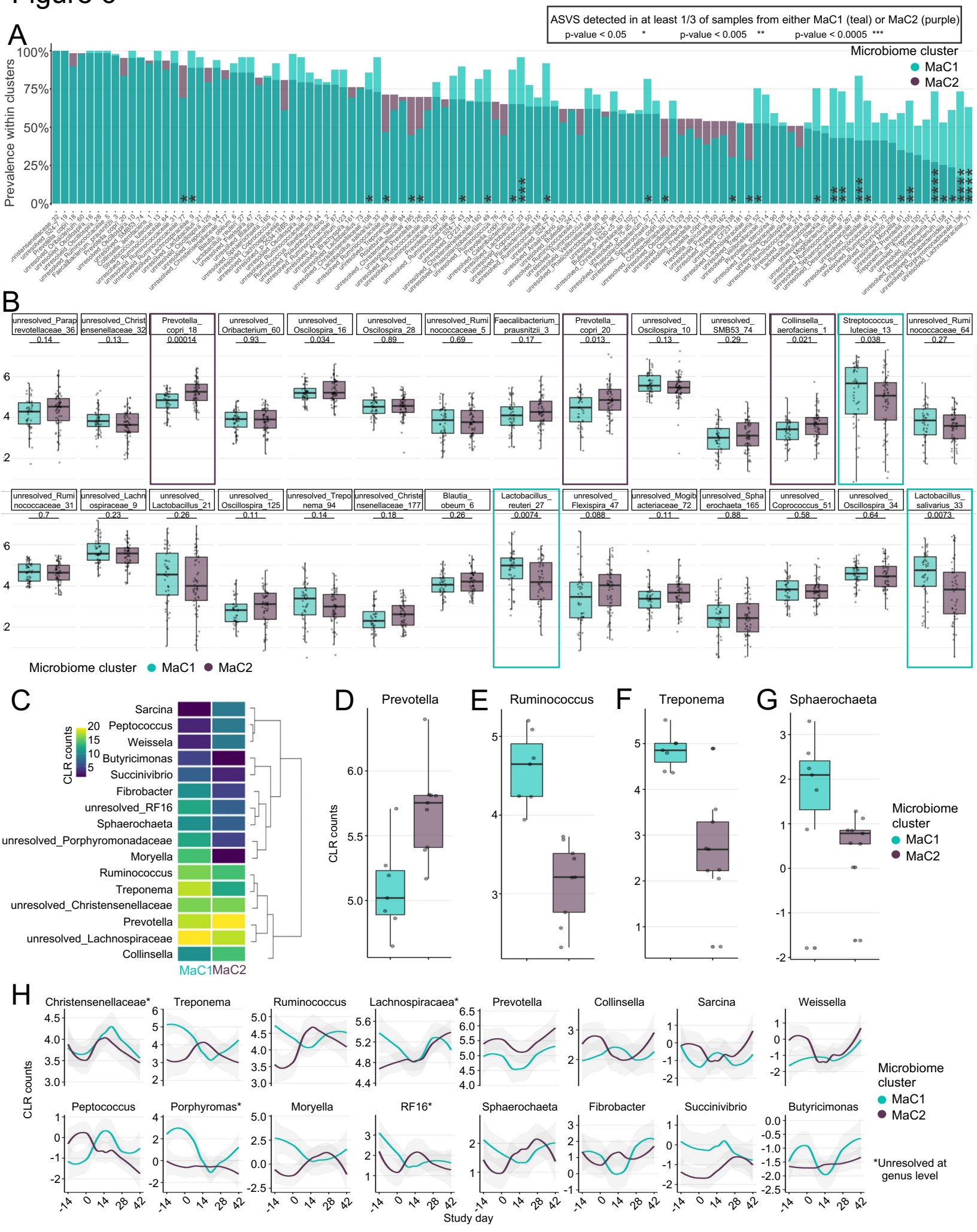
ASVS detected in at least 1/3 of samples from either MaC1 (teal) or MaC2 (purple)
p-value < 0.05 * p-value < 0.005 ** p-value < 0.0005 ***
A
Prevalence within clusters
100%
75%
50%
25%
0%
Microbiome cluster
MaC1
MaC2
B
unresolved_Parabacteroides_36 0.14
unresolved_Christensenellaceae_32 0.13
Prevotella_copri_18 0.00014
unresolved_Oribacterium_60 0.93
unresolved_Oscilospira_16 0.034
unresolved_Oscilospira_28 0.89
unresolved_Ruminococcaceae_5 0.69
Faecalibacterium_prausnitzii_3 0.17
Prevotella_copri_20 0.013
unresolved_Oscilospira_10 0.13
unresolved_SMB53_74 0.29
Collinsella_aerofaciens_1 0.021
Streptococcus_luteciae_13 0.038
unresolved_Ruminococcaceae_64 0.27
unresolved_Ruminococcaceae_31 0.7
unresolved_Lachnospiraceae_9 0.23
unresolved_Lactobacillus_21 0.26
unresolved_Oscillospira_125 0.11
unresolved_Treponema_94 0.14
unresolved_Christensenellaceae_177 0.18
Blautia_obeum_6 0.26
Lactobacillus_reuteri_27 0.0074
unresolved_Flexispira_47 0.088
unresolved_Mogibacteriaceae_72 0.11
unresolved_Sphaerochaeta_165 0.88
unresolved_Coprococcus_51 0.58
unresolved_Oscillospira_34 0.64
Lactobacillus_salivarius_33 0.0073
Microbiome cluster MaC1 MaC2
C
CLR counts
20
15
10
5
Sarcina
Peptococcus
Weissela
Butyricimonas
Succinivibrio
Fibrobacter
unresolved_RF16
Sphaerochaeta
unresolved_Porphyromonadaceae
Moryella
Ruminococcus
Treponema
unresolved_Christensenellaceae
Prevotella
unresolved_Lachnospiraceae
Collinsella
MaC1 MaC2
D Prevotella
E Ruminococcus
F Treponema
G Sphaerochaeta
CLR counts
Microbiome cluster
MaC1
MaC2
H
Christensenellaceae*
Treponema
Ruminococcus
Lachnospiracaea*
Prevotella
Collinsella
Sarcina
Weissella
Peptococcus
Porphyromas*
Moryella
RF16*
Sphaerochaeta
Fibrobacter
Succinivibrio
Butyricimonas
CLR counts
Study day
-14 0 14 28 42
Microbiome cluster
MaC1
MaC2
*Unresolved at genus level

Fig.S1

A

Baseline microbiome hierarchical clusters, individuals colored by KAF156 treatment group

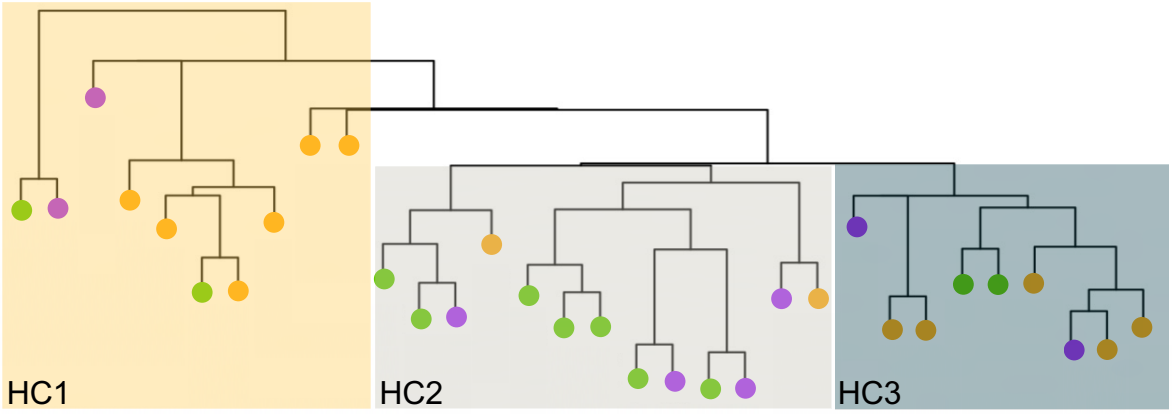

B

Baseline microbiome PCA, individuals colored by KAF156 treatment group

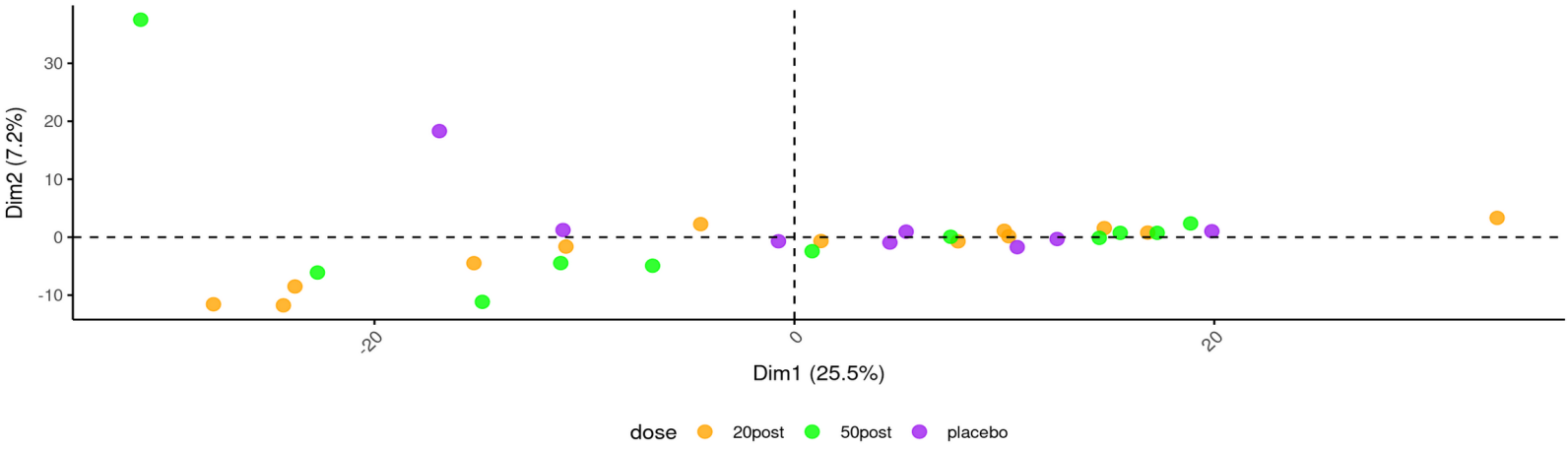

Fig.S2

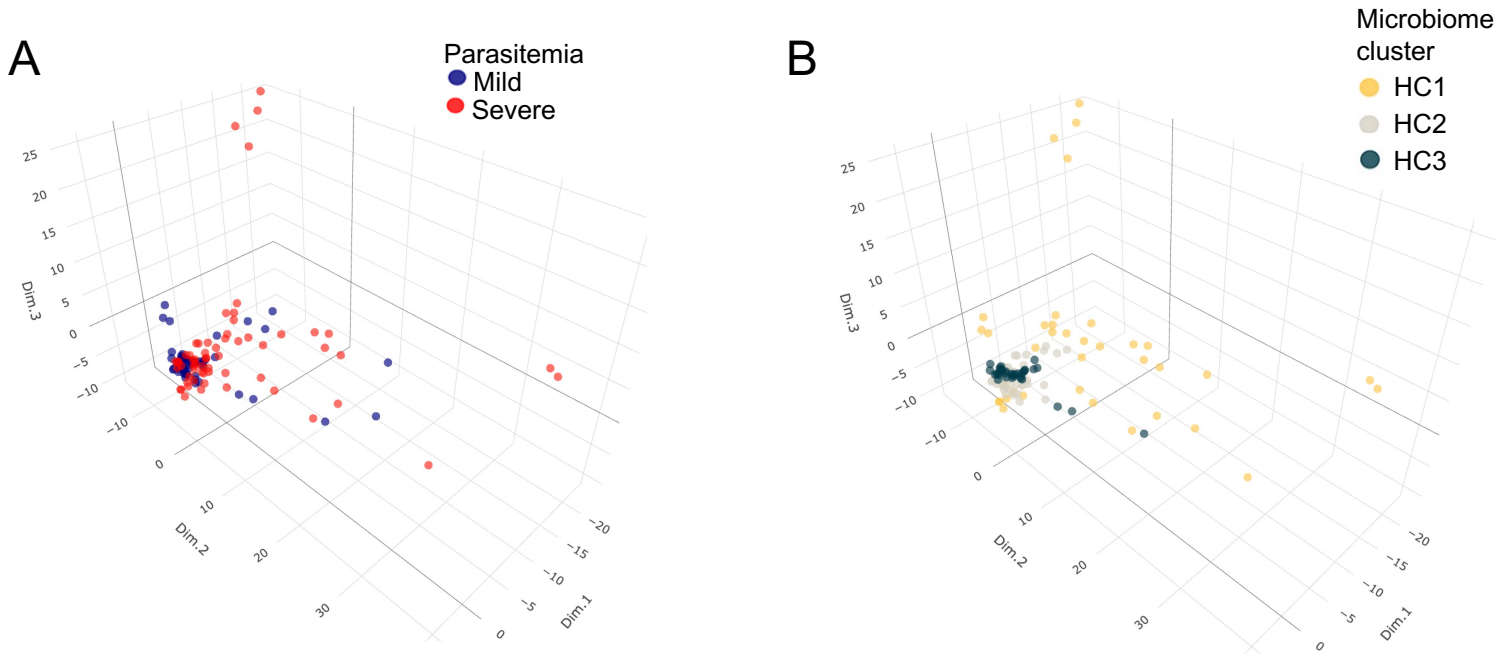
A
Parasitemia
Mild
Severe
Dim.3
Dim.2
Dim.1
B
Microbiome cluster
HC1
HC2
HC3
Dim.3
Dim.2
Dim.1

Fig.S3

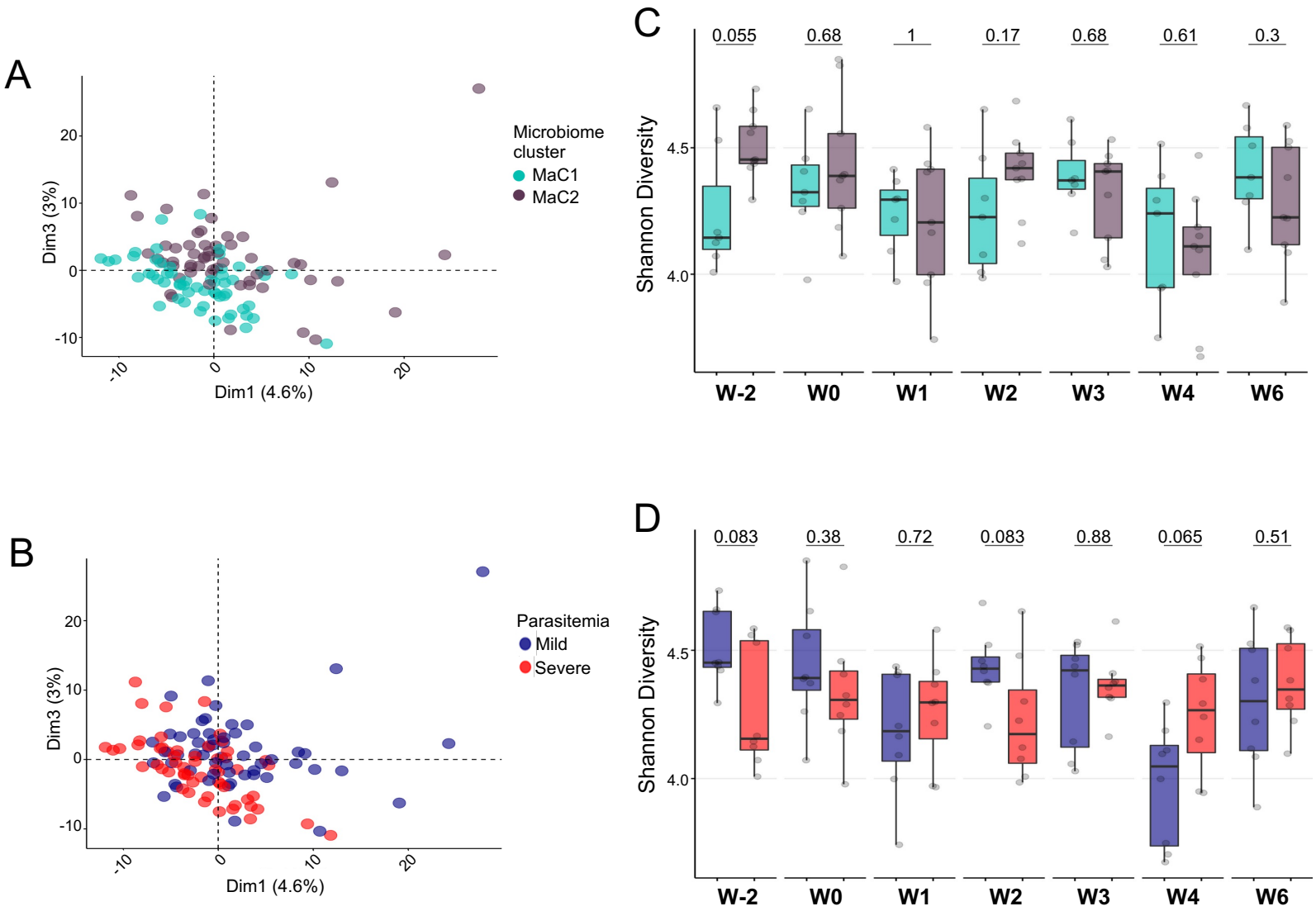
A
Dim3 (3%)
Dim1 (4.6%)
Microbiome cluster
MaC1
MaC2
B
Dim3 (3%)
Dim1 (4.6%)
Parasitemia
Mild
Severe
C
Shannon Diversity
0.055
0.68
1
0.17
0.68
0.61
0.3
W-2
W0
W1
W2
W3
W4
W6
D
Shannon Diversity
0.083
0.38
0.72
0.083
0.88
0.065
0.51
W-2
W0
W1
W2
W3
W4
W6

Fig.S4

A

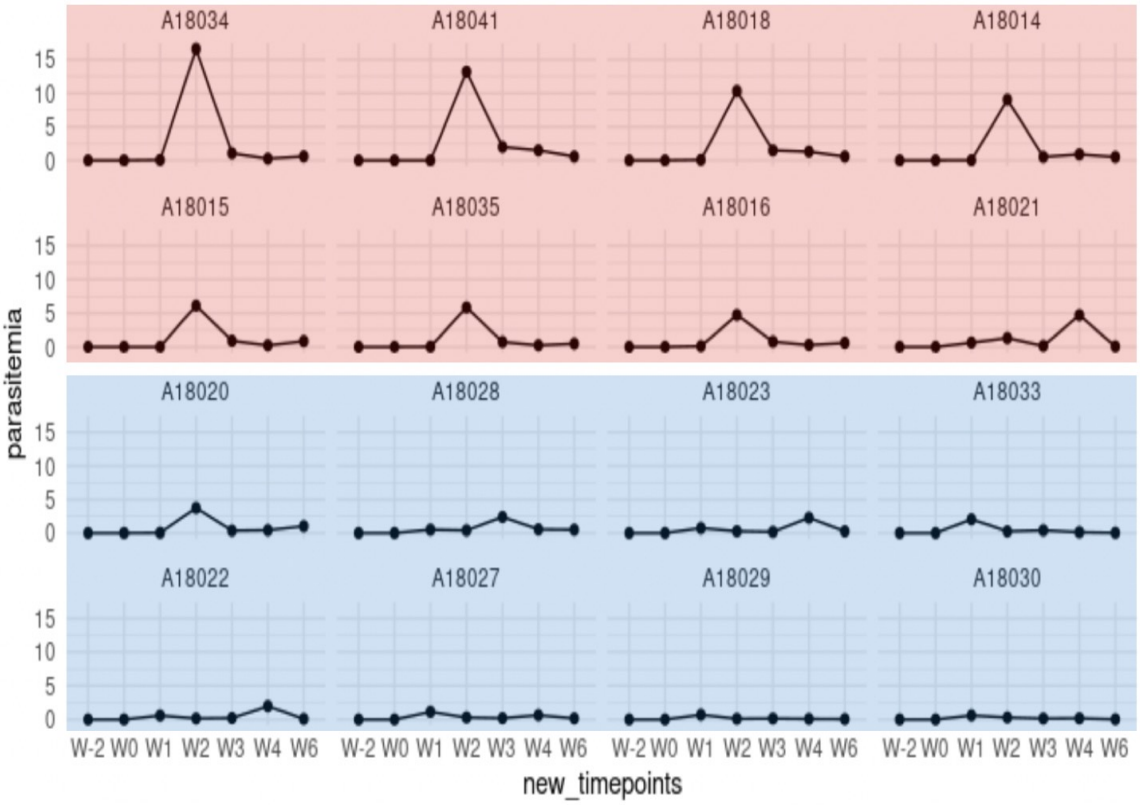
A18034
A18041
A18018
A18014
A18015
A18035
A18016
A18021
A18020
A18028
A18023
A18033
A18022
A18027
A18029
A18030
parasitemia
15
10
5
0
W-2 W0 W1 W2 W3 W4 W6
new_timepoints